applied sciences

MDPI

Article

Investigation of Catalytic Effects and Compositional Variations in Desorption Characteristics of $LiNH_2$-nanoMgH_2

Sesha S. Srinivasan [1,*], Dervis Emre Demirocak [2], Yogi Goswami [3] and Elias Stefanakos [3]

1 Department of Physics, Florida Polytechnic University, 4700 Research Way, Lakeland, FL 33805, USA
2 Department of Mechanical & Industrial Engineering, Texas A&M University-Kingsville, Kingsville, TX 78363, USA; dervis.demirocak@tamuk.edu
3 Clean Energy Research Center, College of Engineering, University of South Florida, Tampa, FL 33620, USA; goswami@usf.edu (Y.G.); estefana@usf.edu (E.S.)
* Correspondence: ssrinivasan@flpoly.org; Tel.: +1-813-451-1876

Received: 9 June 2017; Accepted: 4 July 2017; Published: 7 July 2017

Abstract: $LiNH_2$ and a pre-processed nanoMgH_2 with 1:1 and 2:1 molar ratios were mechano-chemically milled in a high-energy planetary ball mill under inert atmosphere, and at room temperature and atmospheric pressure. Based on the thermogravimetric analysis (TGA) experiments, $2LiNH_2$-nanoMgH_2 demonstrated superior desorption characteristics when compared to the $LiNH_2$-nanoMgH_2. The TGA studies also revealed that doping $2LiNH_2$-nanoMgH_2 base material with 2 wt. % nanoNi catalyst enhances the sorption kinetics at lower temperatures. Additional investigation of different catalysts showed improved reaction kinetics (weight percentage of H_2 released per minute) of the order TiF_3 > nanoNi > nanoTi > nanoCo > nanoFe > multiwall carbon nanotube (MWCNT), and reduction in the on-set decomposition temperatures of the order nanoCo > TiF_3 > nanoTi > nanoFe > nanoNi > MWCNT for the base material $2LiNH_2$-nanoMgH_2. Pristine and catalyst-doped $2LiNH_2$-nanoMgH_2 samples were further probed by X-ray diffraction, Fourier transform infrared spectroscopy, transmission and scanning electron microscopies, thermal programmed desorption and pressure-composition-temperature measurements to better understand the improved performance of the catalyst-doped samples, and the results are discussed.

Keywords: hydrogen storage; complex hydrides; nanocatalyst; $LiNH_2$; MgH_2; ball milling

1. Introduction

The depletion of fossil fuels, especially oil in the near future, rising environmental concerns due to global warming, and the necessity of a secure energy supply have created a worldwide interest in the renewable energy technologies during the last decade. Among many forms of alternative energy options, hydrogen has attracted much attention as an energy carrier due to its potential for the replacement of oil in stationary and mobile applications. However, viable hydrogen storage technology remains the biggest challenge in the utilization of the hydrogen despite intensive research efforts throughout the world. As of now, there is no single material that is capable of attaining the desired set of targets designated by the US Department of Energy (DOE) and FreedomCAR industrial partners. Solid-state hydrogen storage can be broadly classified into two groups considering the mechanisms involved, namely, physisorption, as in carbon-nanotubes (CNT)/metal organic frameworks (MOFs), and chemisorption, as in metal/complex hydrides. The complex metal hydrides, which have been extensively studied recently, have high volumetric and gravimetric densities, but suffer from high desorption temperatures, reversibility, and sluggish kinetics [1]. Therefore, improving the desorption kinetics, reversibility and desorption temperatures of the complex metal hydrides remains a challenge.

Among many complex hydrides investigated, some of the amides (i.e., $LiNH_2/Mg(NH_2)_2$) had shown favorable storage capacity and reversibility.

The studies on the interaction of lithium with hydrogen and nitrogen as early as 1910 led to the discovery of the $LiNH_2$-LiH system [2,3]. However, a detailed investigation of this system as a potential hydrogen storage material was not carried out until 2002 when Chen et al. [4] first reported the promising results for the lithium nitride (Li_3N) system, in which reaction consists of two steps and given as:

$$Li_3N + 2H_2 \leftrightarrow Li_2NH + LiH + H_2 \leftrightarrow LiNH_2 + LiH \quad (1)$$

The theoretical capacity of Li_3N system is 10.4 wt. %; however, only the second step of the reaction path given in (1) is practical for reversible hydrogen storage since the first reaction step has a very low equilibrium pressure (~0.07 bar) [4]. Further investigation of the second step of the reaction (1), which has a theoretical capacity of 6.5 wt. % and favorable thermodynamics, revealed the role of the lithium hydride (LiH). The elementary steps are given by the reaction steps (2) and (3) as follows [5].

$$2LiNH_2 \rightarrow Li_2NH + NH_3 \quad (2)$$

$$NH_3 + LiH \rightarrow LiNH_2 + H_2 \quad (3)$$

The reaction (3) was found to be ultrafast (~25 ms) and responsible for the capture of NH_3 which is detrimental for the fuel cells [5]. After these prolific works, the research on hydrogen storage in amides focused on compositional changes, replacement of Li with other light or more electronegative alkali/earth alkaline metals, mechanical activation, effects of catalysts, reaction mechanism, reversibility issues, and the mitigation of NH_3 emission.

The high desorption temperature (~285 °C at 1 bar) of the $LiNH_2$ + LiH system, which is not feasible for mobile applications, led to studies on the destabilization of the system. One of the ways involves replacing Li with more electronegative metals such as Mg, Na, and Ca. Nakomori et al., partially replaced Li in $LiNH_2$ with 90 at. % Li and 10 at. % Mg, and obtained a 50 K reduction in the desorption temperature [6]. Later, Luo developed a new hydrogen storage material by completely replacing LiH with MgH_2 in the reaction (1). The resulting compound had a 4.5 wt. % gravimetric capacity with a plateau pressure of 30 bar at 200 °C [7]. Further studies on the $LiNH_2$-MgH_2 system concentrated on the reaction mechanism, kinetics, structural characterization, and thermodynamics of the system [8–17]. It was shown that the $2LiNH_2$-MgH_2 system transforms into the $Mg(NH_2)_2$-2LiH system after the first desorption/absorption cycle, and the proposed reaction mechanism is [8,9]:

$$MgH_2 + 2LiNH_2 \rightarrow Li_2Mg(NH)_2 + 2H_2 \leftrightarrow [Mg(NH_2)_2] + 2LiH \quad (4)$$

The different compositions of the Li-Mg-N-H system were also investigated. Leng et al. obtained ~7 wt. % capacity with a $3Mg(NH_2)_2$-8LiH compound, and Nakomori et al. investigated a $3Mg(NH_2)_2$-12LiH compound with a capacity of 9.1 wt. % [18–20]. Despite the higher gravimetric capacities of these systems, desorption temperatures were relatively higher than the $Mg(NH_2)_2$-2LiH compound. Xiong et al. examined the LiH-$Mg(NH_2)_2$ with molar ratios of 1:1, 2:1 and 3:1, and showed that the lower the Li content the higher the NH_3 emission, and the higher the Li content the higher the desorption temperature [21]. A $LiNH_2$-MgH_2 (1:1) compound was also investigated by several researchers, and the results showed considerable NH_3 emission, and the revealed reaction mechanism was quite different than the $LiNH_2$-MgH_2 (2:1) compound [13,22,23].

Besides the Li-N-H and Li-Mg-N-H systems, other (i.e., Li-Ca-N-H) metal amide-metal hydride systems were also investigated. Some researchers focused on the decomposition of metal amides alone to discover new working pairs, and to address the NH_3 emission problem [18–26], whereas some other authors examined the Li-Ca-N-H system, but the results were not superior compared to Li-N-H and Li-Mg-N-H systems [27,28].

Apart from the type of the complex hydride system, the preparation procedure also plays a significant role in the hydrogen storage characteristics of the complex hydrides. The favorable effects of mechanical activation (MA) via ball milling, such as reducing the onset temperature of desorption, enhancing the reaction kinetics, and lowering the activation energy, have been known for a while, and these favorable effects are associated with the creation of nanocrystallites, smaller particle sizes, and increased surface area [29–31]. Regarding the amide systems, MA is especially important in preventing the release of NH_3 by enhancing the homogeneous mixing of the constituents. Since the conversion of amide to imide is an ammonia-mediated process as explained in Equations (2) and (3), a metal hydride compound can effectively capture NH_3 only if the M-amide–M-imide interface could be created at the nanoscale. It was shown that increasing the milling time decreases the grain size monotonically and increases the surface area up to around 5 h milling, as well as enhances the desorption kinetics considerably [30,32–34]. Xie et al. further confirmed that reducing the particle size enhances the reaction kinetics, and reduces the NH_3 emission [35]. Osborn et al., investigated the low temperature milling, and the results showed that desorption kinetics is faster for the sample milled at −196 °C compared to the samples milled at −40 °C and 20 °C [36].

Ammonia emission, even in trace levels, is undesirable in the amide systems because it poisons the fuel cells and causes loss of hydrogen, which in return results in the loss of gravimetric capacity [37]. The effect of NH_3 emission on cyclic behavior and capacity loss is further elaborated, and the results showed that NH_3 emission can be mitigated by ball milling. Ammonia emission is more pronounced for the Li-Mg-N-H system compared to the Li-N-H system since the reaction rate of MgH_2 with NH_3 is slower than the reaction rate between LiH and NH_3 [38–41].

Another important strategy in improving the performance of the complex hydrides is the utilization of catalysts. The seminal study of Bogdanovic on Ti-doped $NaAlH_4$ paved the way for further investigations of the favorable effects of various catalysts in complex hydrides [42]. The favorable effects of catalysts in enhancing the reactions kinetics, lowering the desorption temperature, and alleviating NH_3 emission in the amide systems have been studied by many researchers [43–49]. Ickikawa et al. was the first to investigate the effects of $TiCl_3$, Ni, Co and Fe on NH_3 emission, reaction kinetics, and the desorption temperature of the Li-N-H system, and the results showed that $TiCl_3$ is superior compared to Ni, Co and Fe [39]. Isobe et al. focused on Ti^{nano}, Ti^{micro}, $TiCl_3$, $TiO_2{}^{nano}$, and $TiO_2{}^{micro}$ in the Li-N-H system, and proved the importance of the particle size of the catalysts. The nanocatalysts were superior compared to micro catalysts [44]. Yao et al. investigated Mn, V, MnO_2, and V_2O_5 in the Li-N-H system, and showed that Mn, V, MnO_2, and V_2O_5 has no effect in hydrogen desorption, but enhances the ammonia emission [45]. The catalytic studies on the Li-Mg-N-H system revealed that as-prepared single-wall carbon nanotube (SWCNT) considerably improves the reactions kinetics compared to purified SWCNT/ multiwall carbon nanotube (MWCNT), graphite and activated carbon [46]. Janot et al. [47] showed that Nb_2O_5, $TiCl_3$ and Pd have insignificant effect on kinetics of the Li-Mg-N-H system, and these results were further confirmed elsewhere [48]. Wang et al. reported no improvements on kinetics of the Li-Mg-N-H system using Ti, Fe, Co, Ni, Pd, Pt and their oxides, but they did not disclose the details. However, they showed enhanced kinetics using a potassium-modified $Mg(NH_2)_2$-2LiH compound [49]. Utilization of the transition metal nitrides (TaN, TiN) were also shown to enhance the kinetics [50].

To the best of our knowledge, the effect of various nanocatalysts (i.e., nanoCo, nanoTi, nanoFe, nanoNi, TiF_3 and MWCNT) on the performance of the $LiNH_2$-nanoMgH_2 complex hydride has not been systematically investigated to date. Additionally, we have utilized a preprocessed MgH_2 (nanoMgH_2) in preparation of the $LiNH_2$-nanoMgH_2 complex hydride to better understand the benefits of reduced particle size [51–53]. In this study, the effects of compositional changes on hydrogen storage characteristics of $LiNH_2$-nanoMgH_2 compound has been investigated using (1:1) and (2:1) molar ratios, respectively. The effects of nanoNi catalyst concentration and various other catalysts (i.e., TiF_3, nanoCo, nanoTi, nanoFe and MWCNT) on desorption kinetics, the on-set decomposition temperature, and the gravimetric capacity of the $LiNH_2$-nanoMgH_2 compound are reported.

2. Materials and Methods

$LiNH_2$ was purchased from Sigma-Aldrich, St. Louis, MO, USA, with purity not less than 95%, and MgH_2 was procured from Alfa Aesar (Ward Hill, MA, USA) with a purity of 98%. All the materials were kept and handled in an inert nitrogen atmosphere in a glove box. $LiNH_2$ was used as received, whereas MgH_2 was preprocessed for 15 h in ball mill under Ar/H_2 medium to obtain nanoMgH_2 with finer particle/grain size (<10 nm) compared to as-received MgH_2. The catalyst TiF_3 was purchased from Sigma-Aldrich with 99.9% purity, nanoTi, nanoCo, nanoNi and nanoFe (purity of 90%, particle size range of 3–20 nm, and average surface area of 35–130 m^2/g) were purchased from QuantumSphere Inc. (Santa Ana, CA, USA) and MWCNT (purity of at least 60%) was purchased from Sigma-Aldrich. All the catalysts were used without further purification. The samples were ball milled using an 80 mL stainless steel bowl, which had a custom-built lid to facilitate evacuating/purging with hydrogen/argon (5%/95%) before starting and after every 2 h of ball milling. High-energy ball milling was carried out by Fritsch Pulverisette P6 planetary mill, the ball milling parameters such as the ball-to-powder ratio, milling speed and milling time were to 20:1, 300 RPM and 1–5 h, respectively. The base materials, $xLiNH_2$-MgH_2, were synthesized by milling $xLiNH_2$ (x = 1 or 2) and MgH_2 for 5 h, and then the desired catalysts were added. The resulting compound was ball milled again for 15 min to make sure a thorough dispersion of catalysts in the base materials was obtained. After the ball milling operation, all the samples were kept in a glove box until further characterization as explained below.

The microstructural and chemical analyses were carried out to confirm the morphology and composition of chemical elements by scanning electron microscopy (SEM) and energy dispersive X-rays (EDX). The powder X-ray diffraction (XRD) of the samples was carried out by Philips X'pert diffractometer with CuKα radiation of λ = 1.54060 Å. The as-milled samples were prepared inside the glove box, and sealed with Parafilm® tape, which shows peaks at 2θ angles of 21° and 23°. The diffraction data was analyzed using PANalytical X'pert Highscore software version 1.0f.

The Perkin-Elmer Spectrum One Fourier transform infrared (FTIR) spectrometer was utilized to measure the bond stretches of the complex hydride compound, and the instrument's working range was between 370–7800 cm^{-1} with a resolution of 0.5 cm^{-1}.

The gravimetric weight loss experiments were conducted by TA (New Castle, DE, USA) instrument's SDT-Q600 equipment, which is the combination of thermogravimetric analysis (TGA) and differential scanning calorimetry (DSC). The as-prepared samples and their catalyst doped versions were heated at a rate of 5 °C/min, and the data was analyzed with TA Universal Analysis 2000 software.

The thermal volumetric sorption analyses of the pristine and catalysts loaded base materials were carried out by Setaram (Caluire FRANCE) HyEnergy's PCTPro 2000 (i.e., a fully automated Sievert's type apparatus) and Quantachrome's (Boynton Beach, FL, USA) Autosorb 1C thermal programmed desorption (TPD) equipment.

3. Results and Discussion

3.1. Thermogravmetric Analysis (TGA) and Thermal Programmed Desorption (TPD)

TGA and TPD analyses facilitate the rapid screening of the complex hydride materials in a relatively short duration and gives invaluable information on the desorption characteristics such as gravimetric storage capacity and hydrogen decomposition temperature. To determine the optimal catalyst concentration, we focused on the nanoNi catalyst, which showed enhanced performance in various complex hydrides as discussed in the Introduction. It is highly desirable to use a minimum amount of catalyst to limit the cost of the complex hydride. As shown in Figure S1 (see supplementary information), 2 wt. % nanoNi showed the best desorption performance at temperatures up to 300 °C. Temperatures higher than 300 °C are not practical for the mobile applications; therefore, 2 wt. % nanoNi doping is the optimal catalyst loading for the $2LiNH_2$-nanoMgH_2. The concentration of 2 wt. % nanoNi catalyst was also investigated for the $LiNH_2$-nanoMgH_2 system, and the TGA and TPD results are given in Figures 1 and 2, respectively.

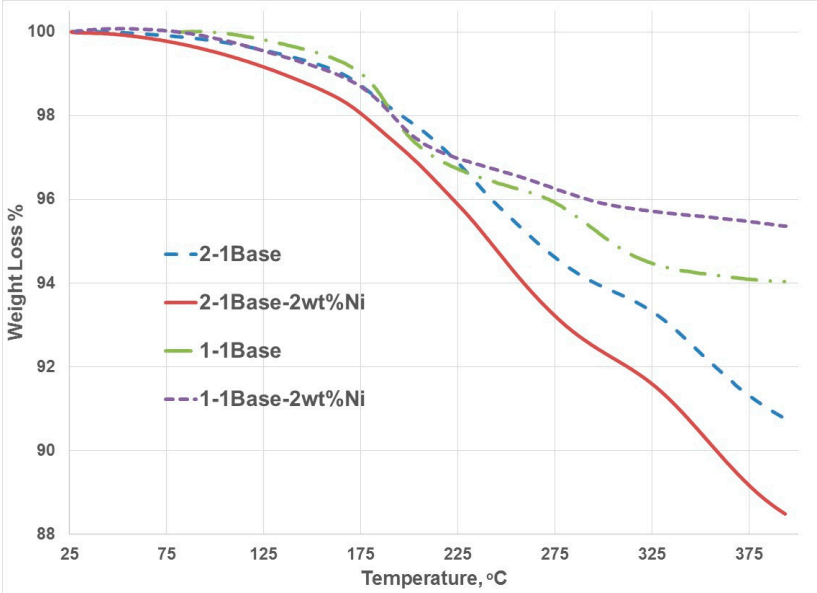

Figure 1. Thermogravimetric analysis (TGA) profiles of pristine and Ni-doped $LiNH_2$-nanoMgH_2 with 1:1 and 2:1 ratios.

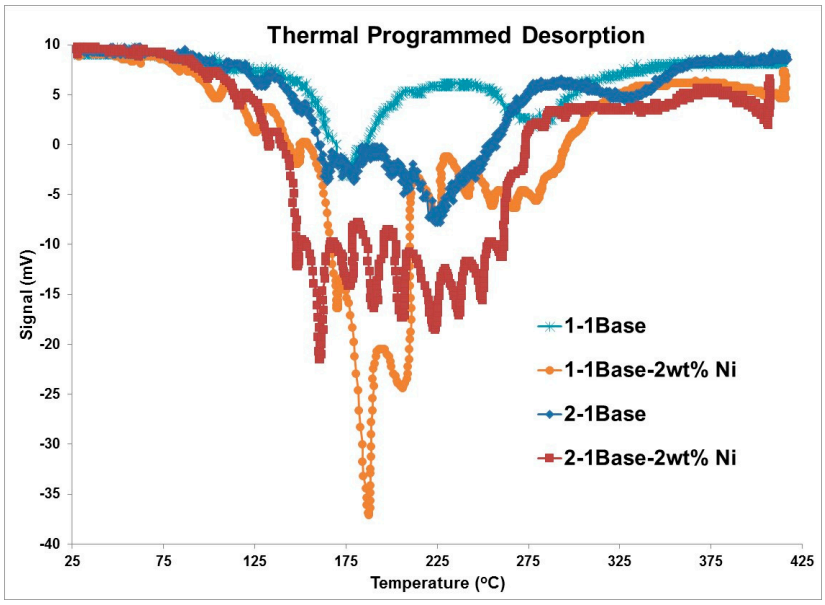

Figure 2. Thermal programmed desorption (TPD) profiles of pristine and 2 wt. % nanoNi-doped $LiNH_2$-nanoMgH_2 with 1:1 and 2:1 ratios.

Considering the TGA results of $LiNH_2$-nanoMgH_2 given in Figure 1, the addition of 2 wt. % nanoNi catalyst improved the hydrogen desorption up until around 200 °C, but hampered the ultimate gravimetric capacity (i.e., capacity at 375 °C) of the $LiNH_2$-nanoMgH_2 system. This result is in line with TPD studies. According to Figure 2, the hydrogen signal of the 2 wt. % nanoNi-doped $LiNH_2$-nanoMgH_2 increases up until 200 °C during the TPD experiments, then sharply decreases with increasing temperatures. From the practical application point of view, high temperature performance of the complex hydrides is not critical for the mobile applications; therefore, it is concluded that nanoNi doping is desirable for the $LiNH_2$-nanoMgH_2 system.

Regarding the TGA of $2LiNH_2$-nanoMgH_2 material given in Figure 1, the 2 wt. % nano-Ni doping enhances the gravimetric capacity of the base material at all temperatures studied. The TPD

results given in Figure 2, however, show stronger hydrogen desorption signal for 2 wt. % nanoNi added material compared to the base material, which is further evidence for higher H_2 desorption from 2 wt. % nanoNi-doped material. Comparing gravimetric capacities of $LiNH_2$-MgH_2 with the molar ratios of 1:1 and 2:1 given in Figures 1 and 2, the $2LiNH_2$-nanoMgH_2 compound is superior to $LiNH_2$-nanoMgH_2, hence $2LiNH_2$-nanoMgH_2 is selected for further investigation.

A closer look into Figures 1 and 2 on the thermogravimetric and thermal programmed desorption profiles of 2 wt. % nanoNi-doped $LiNH_2$-nanoMgH_2 with 1:1 and 2:1 ratios are discussed here. The TGA of the 2 wt. % doped 1:1 sample shows the gaseous weight loss close to 5% with two desorption steps, whereas the 2 wt. % nanoNi-doped 2:1 sample shows double the weight loss capacity (~10%) with single major decomposition step and inflections at higher temperatures (~325 °C). This is confirmed from the TPD profile (Figure 2) of 2 wt. % doped 2:1 compound, where the total effective desorption or decomposition attributed in a single broader step when compared to TPD profiles of 2 wt. % doped 1:1 $LiNH_2$-nanoMgH_2 compound, where there are two sharp decomposition steps below 225 °C. We have also demonstrated TGA with other nickel concentrations, and found that lower nanoNi catalyst concentration of 2 wt. % is ideal to improve the gaseous hydrogen decomposition characteristics such storage capacity and the rate of desorption (see Supplementary Material Figure S1).

The TGA and TPD results of mixing 2 wt. % nanoNi, nanoCo, nanoFe, nanoTi and TiF_3 are given in Figures 3 and 4, respectively. Thus, these catalysts enhance the hydrogen desorption kinetics as well as the gravimetric capacity in comparison to the base material.

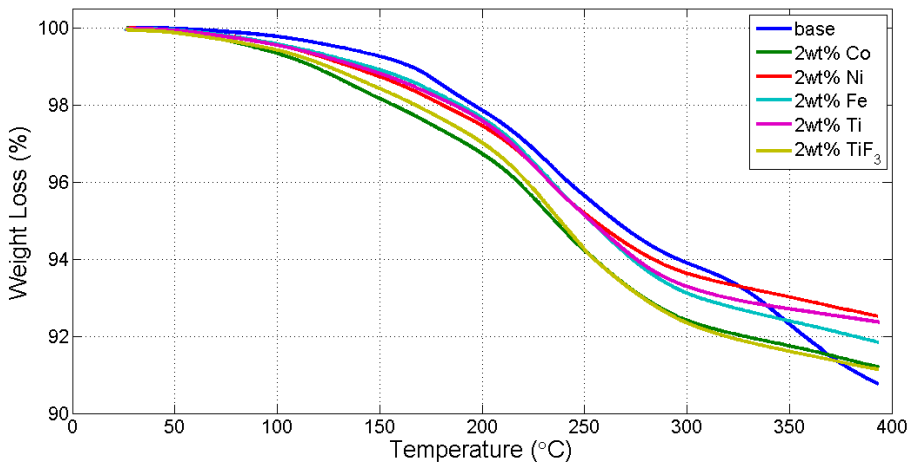

Figure 3. TGA analysis of the different catalysts on $LiNH_2$-nanoMgH_2 (2:1).

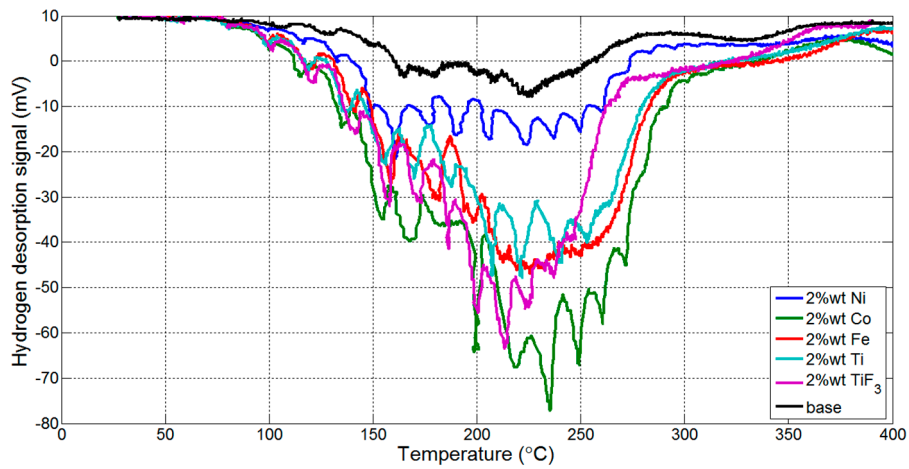

Figure 4. TPD characteristics of different catalysts on $LiNH_2$-nanoMgH_2 (2:1) from TPD analysis.

A closer analysis on the linear portion and start-up on-set point on the profiles of Figure 3, the reaction kinetics (wt. %/min) and on-set decomposition temperature were estimated for all the catalysts and are summarized in Table 1. It can been seen from Table 1 that TiF_3 enhances the reaction kinetics most with the order of TiF_3 > nanoNi > nanoTi > nanoCo > nanoFe, and the highest reduction in on-set desorption temperature was obtained from the nanoCo catalyst (nanoCo > TiF_3 > nanoTi > nanoFe > nanoNi).

Table 1. Reaction kinetics and on-set decomposition temperature of $2LiNH_2$-nanoMgH_2 with different catalysts.

Reaction Kinetics (wt. %/min)		On-Set Temperature (°C)	
TiF_3	0.5816	nanoCo	121.96
nanoNi	0.5330	TiF_3	125.99
nanoTi	0.5312	nanoTi	136.65
nanoCo	0.5255	nanoFe	142.86
nanoFe	0.5113	nanoNi	149.30

The thermal programed desorption profiles, unlike TGA, may only provide insights into the decomposition temperature along with strength of signal indicating the concentration of gaseous decomposition. Therefore, the trend in reaction kinetics as obtained from TGA in Figure 3 above may not be comparable to the TPD profiles of Figure 4. It seems, however, that the TPD of nanoCo excelled in the highest hydrogen concentration with the order of nanoCo > TiF_3 > nanoFe = nanoTi > nanoNi > base. By comparing the TGA profiles at an instant decomposition temperature say 225 °C, it is discernible again that nanoCo and TiF_3 outperformed with highest hydrogen release capacity and then continues with the order nanoCo > TiF_3 > nanoFe = nanoTi = nanoNi > base. Overall, the catalyst-doped $2LiNH_2$-MgH_2 thus enhances the hydrogen decomposition kinetics while maintaining available hydrogen content similar to that of the base hydride compound. The high reactivity of cobalt nanoparticles and the Ti^{3+} state of TiF_3 thus increases the reaction kinetics for the hydrogen absorption and reversible desorption. Further research is needed to understand why only Co among all transition metal nanoparticles (Fe, Ti, Ni) is superior in hydrogen decomposition at low temperatures.

3.2. Desorption Kinetics Using Sievert's Type Measurements

The ramping desorption kinetics (1 °C/min) of the base material $2LiNH_2$-MgH_2 and 2 wt. % Ni-added $2LiNH_2$-MgH_2 compound are given in Figure 5. As expected, Ni addition did not alter the overall desorption capacity of $2LiNH_2$-MgH_2 since the final desorption temperature was 325 °C. However, Ni addition showed enhanced kinetics and higher desorption capacity up to 250 °C.

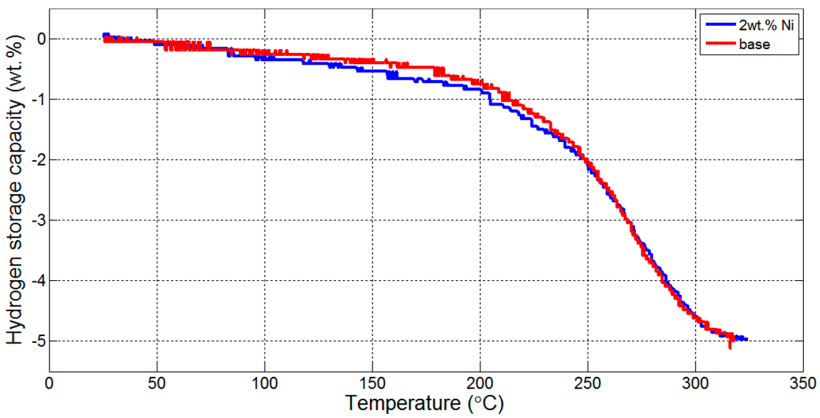

Figure 5. Ramping kinetics of $2LiNH_2$-nanoMgH_2 and $2LiNH_2$-nanoMgH_2 + 2 wt. % Ni.

The absorption kinetics of 2 wt. % Ni added $2LiNH_2$-MgH_2 and the base material $2LiNH_2$-MgH_2 at 180, 200, and 220 °C are given in Figure 6 The catalyst-added compound performed best in terms of kinetics at 200 °C, reaching 2.6 wt. % capacity in 60 min, whereas the base material can only reach a capacity of 1.75 wt. % in 60 min, as shown in Figure 6. The absorption kinetics of 2 wt. % Ni added $2LiNH_2$-MgH_2 at 180, 200, and 220 °C up to 5 h is also given in Figure S2 (see Supplementary Material). The ultimate capacity of 2 wt. % Ni-added $2LiNH_2$-MgH_2 is around 3.5 wt. % at 200 °C (Figure S2), which is lower than the theoretical and reported values earlier [41]. This discrepancy is due to differences in the material preparation procedure, slightly different compound ratios ($LiNH_2$ to MgH_2 ratio is 2:1 in this study as compared to 2:1.1 in Ref [41]), NH_3 emission, and the self-decomposition of $Mg(NH_2)_2$ to Mg_3N_2 at elevated temperatures. Among these, the self-decomposition of $Mg(NH_2)_2$ to Mg_3N_2 is considered to be the main reason, since every absorption cycle preceded by the evacuation of the $2LiNH_2$-MgH_2 compound at 325 °C for 60 min to make sure for the complete desorption of the sample. Moreover, the self-decomposition of $Mg(NH_2)_2$ to Mg_3N_2 was also confirmed with the XRD measurements, as explained in Section 3.3.

On the other hand, Luo et al. showed a 25% capacity loss after 270 cycles where 7% of the capacity loss was attributed to NH_3 emission that increases with higher desorption temperatures [41]. Since the desorption temperature in this study was much higher (325 °C compared to 240 °C in Ref [41]), the main reasons for the apparent capacity loss are twofold: self-decomposition of $Mg(NH_2)_2$ to Mg_3N_2, and NH_3 emission. Therefore, high temperatures should be avoided in utilization of the $2LiNH_2$-MgH_2 compound. To better understand the capacity loss due to self-decomposition of $Mg(NH_2)_2$ to Mg_3N_2 and NH_3 emission, further investigations are underway by utilizing gas chromatography and a residual gas analyzer coupled with a quadruple mass-spectrometer.

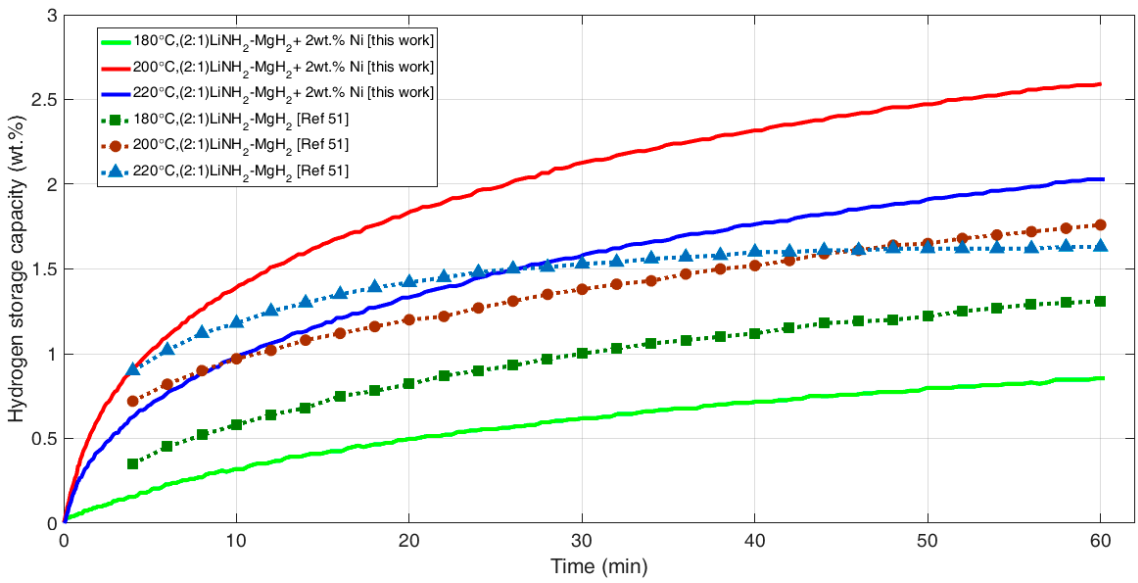

Figure 6. Absorption kinetics of $2LiNH_2$-nanoMgH_2 + 2 wt. % Ni and the base material $2LiNH_2$-MgH_2 at 180, 200, and 220 °C [54].

It is well known that the addition of transition metal catalysts to complex hydrides does not change the thermodynamic properties (i.e., enthalpy of formation) of the base material, but enhances the kinetic properties of the base material by lowering the activation energy [55]. The exact mechanism for the improved kinetics by Ni addition is not well understood currently. However, the enhanced kinetics due to Ni addition is considered to be associated with the increased heterogeneous sites for the nucleation of the complex hydride phases given in Equation (4). Additionally, Ni addition can facilitate the hydrogen diffusion through the complex hydride matrix [56].

3.3. X-ray Diffraction (XRD), Fourier Transform Infrared Spectroscopy (FTIR) Scanning Electron Microscopy (SEM), and Energy Dispersive X-rays (EDX)

The conversion or yield of the products have been determined by metrological characterization tools such as X-ray diffraction for phase identification, FTIR spectroscopic analysis for chemical bonding information, and SEM/EDX microscopic tools to evaluate the microstructure and nanoparticle size determination in addition to compositional (elemental) distributions.

X-ray diffraction and Fourier transform infrared spectroscopy were employed to characterize the $2LiNH_2$-MgH_2 compound after ball milling (BM), and after pressure composition temperature (PCT) measurements in hydrogenated/dehydrogenated conditions, to verify the validity of the reaction mechanism given in reaction (3). FTIR spectra of $LiNH_2$, $2LiNH_2$-MgH_2 after 5 h ball milling (BM) and after PCT measurements in hydrogenated/dehydrogenated conditions are given in Figure 7. The characteristics of N-H asymmetric and symmetric vibrations of $LiNH_2$ at 3313 and 3259 cm^{-1}, respectively, were observed in $2LiNH_2$-MgH_2 after 5 h BM. FTIR spectrum of hydrogenated $2LiNH_2$-MgH_2 showed the characteristic bands of $Mg(NH_2)_2$ at 3278 and 3325 cm^{-1} and Mg_3N_2 band at 3160 cm^{-1} [10,57]. On the other hand, the FTIR spectrum of the fully dehydrogenated $2LiNH_2$-MgH_2 showed the characteristic peaks of $Li_2Mg(NH)_2$ compound at 3163 and 3180 cm^{-1} [38].

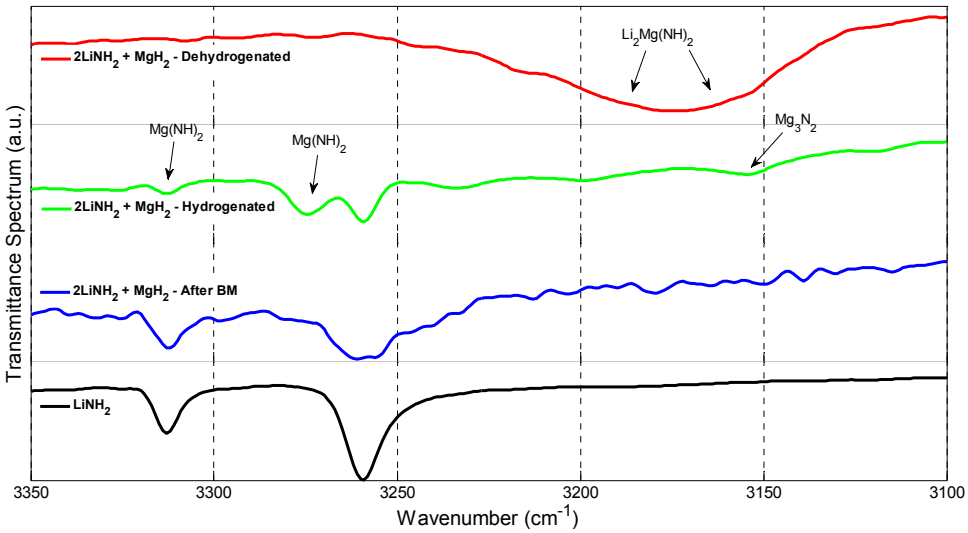

Figure 7. Fourier transform infrared spectroscopy (FTIR) spectra of $LiNH_2$-nanoMgH_2 (2:1) before and after pressure composition temperature (PCT).

The XRD profiles of the empty sample holder, $2LiNH_2$-MgH_2 after 5 h BM and after PCT measurements in hydrogenated/dehydrogenated conditions, are given in Figure 8. Self-decomposition of $Mg(NH_2)_2$ to Mg_3N_2 at elevated temperatures was discussed by Luo et al., and further proved unambiguously by XRD and FTIR measurements in this study [41]. However, the XRD of the dehydrogenated sample resulted in an unidentified peak around 27.5° which needs to be further investigated. This peak could be the result of an oxide formation at high desorption temperatures due to the impurities in the as-received raw materials. The SEM/EDX mapping and image of the of $2LiNH_2$-MgH_2 + 2 wt. % Ni is given in Figure 9, which clearly shows the uniform dispersion of nanoNi particles among the $2LiNH_2$-MgH_2 compound. Therefore, 15 min is a reasonable duration for mixing catalyst with the base material. Moreover, the EDX spectral analysis of these samples demonstrated the correct 2 wt. % fraction of elemental Ni catalyst on a base hydride matrix. Additionally, the morphology and particles size of the nanoNi (obtained from QuantumSphere Inc.) catalyst was determined by the transmission electron microscopy (TEM), and is shown in Figure 10. From the TEM microstructure, it is evidenced that we have used cluster sizes of 3–10 nm nickel nanoparticles admixed with the base hydride compound that has enhanced hydrogen absorption and desorption kinetics.

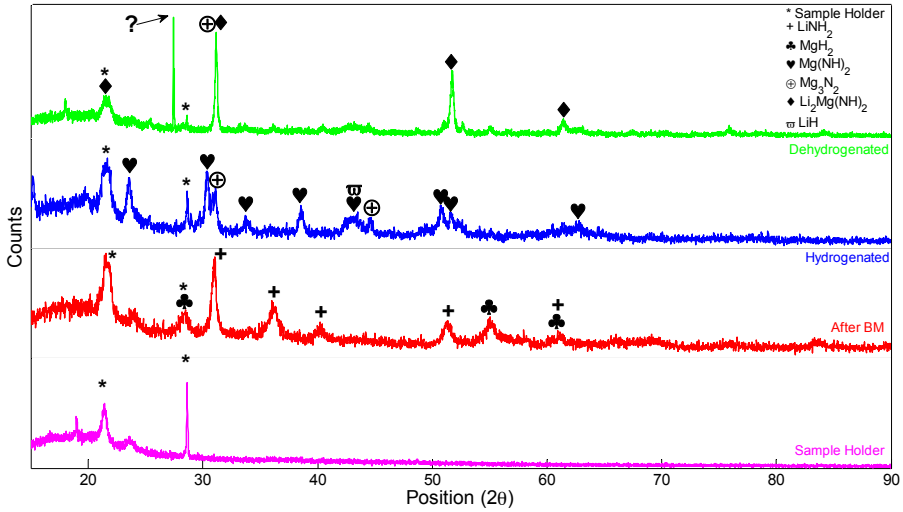

Figure 8. X-ray diffraction (XRD) spectra of $LiNH_2$-nanoMgH_2 after ball milling and after PCT measurements in hydrogenated/dehydrogenated states.

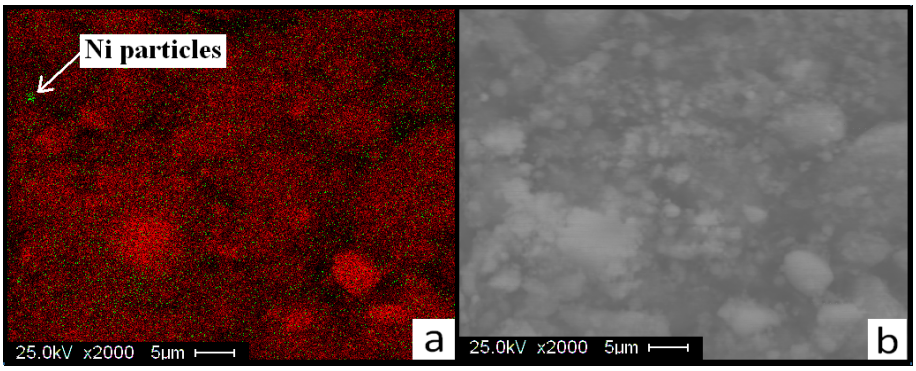

Figure 9. Scanning electron microscopy (SEM)/ energy dispersive X-rays (EDX) mapping (**a**) and image (**b**) of the $2LiNH_2$-nanoMgH_2 + 2 wt. % Ni. Red and green color (labeled) represents Mg and Ni, respectively.

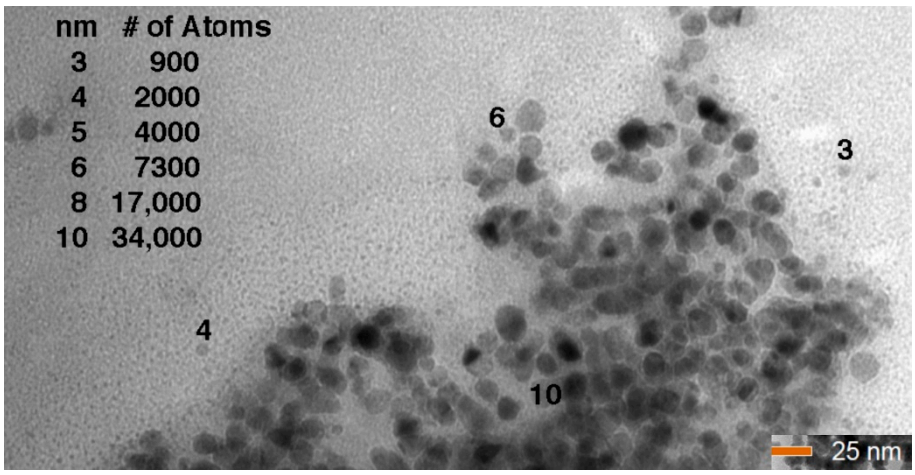

Figure 10. Transmission electron microscopy (TEM) image of nickel nanopartile manufactured by the QuatumSphere Inc. [58].

4. Conclusions

The complex hydride $LiNH_2$-nanoMgH_2 compound was systematically investigated considering different compositional variations and the effect of various catalysts. The thermogravimetric and thermal programmed desorption results revealed that $2LiNH_2$-nanoMgH_2 has higher hydrogen storage capacity and faster sorption kinetics when compared to $LiNH_2$-nanoMgH_2. Among the various concentrations of nanoNi additives on the base material of $2LiNH_2$-nanoMgH_2, 2 wt. % nanoNi showed enhancement in reaction kinetics. Additionally, the TiF_3 doping demonstrates greater reaction kinetics (0.5816 wt. %/min), whereas the nanoCo doping shows the lowest on-set decomposition temperature (121.96 °C) as obtained from the TGA results. The absorption kinetics of $2LiNH_2$-MgH_2 mixed with 2 wt. % nanoNi was rapid at 200 °C, and more than a twofold increase in kinetics when compared to the base material within the first 60 min of absorption. Structural, microstructural, and chemical investigations using metrological tools further supported that high temperature desorption is detrimental to the overall capacity of the $2LiNH_2$-MgH_2 compound.

Supplementary Materials: The following are available online at http://www.mdpi.com/2076-3417/7/7/701/s1, Figure S1: TGA analysis of Ni doped $LiNH_2$-nanoMgH_2 (2:1); Figure S2: Absorption kinetics of $2LiNH_2$-nanoMgH_2 + 2 wt. % Ni at 180, 200 and 220 °C.

Acknowledgments: The authors wish to acknowledge the Florida Energy Systems Consortium (FESC) and US Department of Energy for the project funding and support.

Author Contributions: Sesha S. Srinivasan and Dervis Emre Demirocak conceived and designed the experiments; Sesha S. Srinivasan and Dervis Emre Demirocak performed the experiments; Yogi Goswami and Elias Stefanakos analyzed the data; Sesha S. Srinivasan and Dervis Emre Demirocak wrote the paper. Elias Stefanakos and Yogi Goswami proofread the manuscript.

Conflicts of Interest: The authors declare no conflict of interest.

Abbreviations

BM	Ball Milling
CNT	Carbon Nanotube
DSC	Differential Scanning Calorimetry
DOE	Department of Energy
EDX	Energy Dispersive X-rays
FTIR	Fourier Transform Infrared Spectroscopy
MA	Mechanical Activation
MOF	Metal Organic Frameworks
MWCNT	Multiwall Carbon Nanotube
PCT	Pressure Composition Temperature
RPM	revolutions per minute
SDT	Simultaneous TGA and DSC
SEM	Scanning Electron Microscopy
SWCNT	Single Wall Carbon Nanotube
TCD	Thermal Conductivity Detector
TEM	Transmission Electron Microscopy
TGA	Thermogravimetric Analysis
TPD	Thermal Program Desorption
wt. %	weight percent
XRD	X-Ray Diffraction

References

1. Orimo, S.; Nakamori, Y.; Eliseo, J.R.; Zuettel, A.; Jensen, C.M. Complex hydrides for hydrogen storage. *Chem. Rev.* **2007**, *107*, 4111–4132. [CrossRef] [PubMed]
2. Dafert, F.; Miklauz, R. New compounds of nitrogen and hydrogen with lithium. *Monatsh. Chem.* **1910**, *31*, 981. [CrossRef]

3. Ruff, O.; Goeres, H. Li imide and some compounds of N, H and Li. *Ber. Dtsch. Chem. Ges.* **1910**, *44*, 502–506. [CrossRef]
4. Chen, P.; Xiong, Z.; Luo, J.; Lin, J.; Tan, K.L. Interaction of hydrogen with metal nitrides and imides. *Nature* **2002**, *420*, 302–304. [CrossRef] [PubMed]
5. Hu, Y.H.; Ruckenstein, E. Ultrafast reaction between LiH and NH_3 during H_2 storage in Li_3N. *J. Phys. Chem. A* **2003**, *107*, 9737–9739. [CrossRef]
6. Nakamori, Y.; Orimo, S. Destabilization of Li-based complex hydrides. *J. Alloys Compd.* **2004**, *370*, 271–275. [CrossRef]
7. Luo, W. ($LiNH_2$-MgH_2): A viable hydrogen storage system. *J. Alloys Compd.* **2004**, *381*, 284–287. [CrossRef]
8. Luo, W.; Rönnebro, E. Towards a viable hydrogen storage system for transportation application. *J. Alloys Compd.* **2005**, *404*, 392–395. [CrossRef]
9. Xiong, Z.; Wu, G.; Hu, J.; Chen, P. Ternary imides for hydrogen storage. *Adv. Mater.* **2004**, *16*, 1522–1525. [CrossRef]
10. Luo, W.; Sickafoose, S. Thermodynamic and structural characterization of the Mg-Li-NH hydrogen storage system. *J. Alloys Compd.* **2006**, *407*, 274–281. [CrossRef]
11. Lohstroh, W.; Fichtner, M. Reaction steps in the Li-Mg-NH hydrogen storage system. *J. Alloys Compd.* **2007**, *446*, 332–335. [CrossRef]
12. Chen, Y.; Wu, C.Z.; Wang, P.; Cheng, H.M. Structure and hydrogen storage property of ball-milled $LiNH_2/MgH_2$ mixture. *Int. J. Hydrog. Energy* **2006**, *31*, 1236–1240. [CrossRef]
13. Pottmaier, D.; Dolci, F.; Orlova, M.; Vaughan, G.; Fichtner, M.; Lohstroh, W.; Baricco, M. Hydrogen release and structural transformations in $LiNH_2$-MgH_2 systems. *J. Alloys Compd.* **2010**, *509*, 719–723. [CrossRef]
14. Chen, P.; Xiong, Z.; Yang, L.; Wu, G.; Luo, W. Mechanistic investigations on the heterogeneous solid-state reaction of magnesium amides and lithium hydrides. *J. Phys. Chem. B* **2006**, *110*, 14221–14225. [CrossRef] [PubMed]
15. Wang, J.; Li, H.; Wang, S.; Liu, X.; Li, Y.; Jiang, L. The desorption kinetics of the $Mg(NH_2)_2$ + LiH mixture. *Int. J. Hydrog. Energy* **2009**, *34*, 1411–1416. [CrossRef]
16. Yang, J.; Sudik, A.; Wolverton, C. Activation of hydrogen storage materials in the Li-Mg-NH system: Effect on storage properties. *J. Alloys Compd.* **2007**, *430*, 334–338. [CrossRef]
17. Xiong, Z.; Hu, J.; Wu, G.; Chen, P.; Luo, W.; Gross, K.; Wang, J. Thermodynamic and kinetic investigations of the hydrogen storage in the Li-Mg-NH system. *J. Alloys Compd.* **2005**, *398*, 235–239. [CrossRef]
18. Leng, H.; Ichikawa, T.; Hino, S.; Hanada, N.; Isobe, S.; Fujii, H. New metal-NH system composed of $Mg(NH_2)_2$ and LiH for hydrogen storage. *J. Phys. Chem. B* **2004**, *108*, 8763–8765. [CrossRef]
19. Nakamori, Y.; Kitahara, G.; Miwa, K.; Towata, S.; Orimo, S. Reversible hydrogen-storage functions for mixtures of Li_3N and Mg_3N_2. *Appl. Phys. A Mater. Sci. Process.* **2005**, *80*, 1–3. [CrossRef]
20. Leng, H.; Ichikawa, T.; Fujii, H. Hydrogen Storage Properties of Li-Mg-N-H Systems with Different Ratios of $LiH/Mg(NH_2)_2$. *J. Phys. Chem. B* **2006**, *110*, 12964–12968. [CrossRef] [PubMed]
21. Xiong, Z.; Wu, G.; Hu, J.; Chen, P.; Luo, W.; Wang, J. Investigations on hydrogen storage over Li-Mg-NH complex-the effect of compositional changes. *J. Alloys Compd.* **2006**, *417*, 190–194. [CrossRef]
22. Osborn, W.; Markmaitree, T.; Shaw, L.L. Evaluation of the hydrogen storage behavior of a $LiNH_2$ + MgH_2 system with 1:1 ratio. *J. Power Sources* **2007**, *172*, 376–378. [CrossRef]
23. Leng, H.; Ichikawa, T.; Hino, S.; Hanada, N.; Isobe, S.; Fujii, H. Synthesis and decomposition reactions of metal amides in metal-NH hydrogen storage system. *J. Power Sources* **2006**, *156*, 166–170. [CrossRef]
24. Lu, J.; Choi, Y.J.; Fang, Z.Z.; Sohn, H.Y. Effect of milling intensity on the formation of LiMgN from the dehydrogenation of $LiNH_2$-MgH_2 (1:1) mixture. *J. Power Sources* **2010**, *195*, 1992–1997. [CrossRef]
25. Leng, H.; Ichikawa, T.; Isobe, S.; Hino, S.; Hanada, N.; Fujii, H. Desorption behaviours from metal-NH systems synthesized by ball milling. *J. Alloys Compd.* **2005**, *404*, 443–447. [CrossRef]
26. Pinkerton, F. Decomposition kinetics of lithium amide for hydrogen storage materials. *J. Alloys Compd.* **2005**, *400*, 76–82. [CrossRef]
27. Tokoyoda, K.; Hino, S.; Ichikawa, T.; Okamoto, K.; Fujii, H. Hydrogen desorption/absorption properties of Li-Ca-NH system. *J. Alloys Compd.* **2007**, *439*, 337–341. [CrossRef]
28. Chu, H.; Xiong, Z.; Wu, G.; He, T.; Wu, C.; Chen, P. Hydrogen storage properties of Li-Ca-NH system with different molar ratios of $LiNH_2/CaH_2$. *Int. J. Hydrog. Energy* **2010**, *35*, 8317–8321. [CrossRef]

29. Zaluska, A.; Zaluski, L.; Ström-Olsen, J. Structure, catalysis and atomic reactions on the nano-scale: A systematic approach to metal hydrides for hydrogen storage. *Appl. Phys. A Mater. Sci. Process.* **2001**, *72*, 157–165. [CrossRef]
30. Markmaitree, T.; Ren, R.; Shaw, L.L. Enhancement of lithium amide to lithium imide transition via mechanical activation. *J. Phys. Chem. B* **2006**, *110*, 20710–20718. [CrossRef] [PubMed]
31. Liu, Y.; Zhong, K.; Luo, K.; Gao, M.; Pan, H.; Wang, Q. Size-Dependent Kinetic Enhancement in Hydrogen Absorption and Desorption of the Li-Mg-N-H System. *J. Am. Chem. Soc.* **2009**, *131*, 1862–1870. [CrossRef] [PubMed]
32. Varin, R.; Jang, M.; Polanski, M. The effects of ball milling and molar ratio of LiH on the hydrogen storage properties of nanocrystalline lithium amide and lithium hydride ($LiNH_2$ + LiH) system. *J. Alloys Compd.* **2010**, *491*, 658–667. [CrossRef]
33. Shaw, L.L.; Ren, R.; Markmaitree, T.; Osborn, W. Effects of mechanical activation on dehydrogenation of the lithium amide and lithium hydride system. *J. Alloys Compd.* **2008**, *448*, 263–271. [CrossRef]
34. Shahi, R.R.; Yadav, T.; Shaz, M.; Srivastava, O. Effects of mechanical milling on desorption kinetics and phase transformation of $LiNH_2/MgH_2$ mixture. *Int. J. Hydrog. Energy* **2008**, *33*, 6188–6194. [CrossRef]
35. Xie, L.; Liu, Y.; Li, G.; Li, X. Improving Hydrogen Sorption Kinetics of the $Mg(NH_2)_2$-LiH System by the Tuning Particle Size of the Amide. *J. Phys. Chem. C* **2009**, *113*, 14523–14527. [CrossRef]
36. Osborn, W.; Markmaitree, T.; Shaw, L.L.; Hu, J.Z.; Kwak, J.H.; Yang, Z. Low temperature milling of the $LiNH_2$ + LiH hydrogen storage system. *Int. J. Hydrog. Energy* **2009**, *34*, 4331–4339. [CrossRef]
37. Ikeda, S.; Kuriyama, N.; Kiyobayashi, T. Simultaneous determination of ammonia emission and hydrogen capacity variation during the cyclic testing for $LiNH_2$-LiH hydrogen storage system. *Int. J. Hydrog. Energy* **2008**, *33*, 6201–6204. [CrossRef]
38. Markmaitree, T.; Osborn, W.; Shaw, L.L. Comparisons between MgH_2- and LiH-containing systems for hydrogen storage applications. *Int. J. Hydrog. Energy* **2008**, *33*, 3915–3924. [CrossRef]
39. Markmaitree, T.; Osborn, W.; Shaw, L.L. Comparative studies of reaction rates of NH_3 with MgH_2 and LiH. *J. Power Sources* **2008**, *180*, 535–538. [CrossRef]
40. Luo, W.; Stewart, K. Characterization of NH_3 formation in desorption of Li-Mg-NH storage system. *J. Alloys Compd.* **2007**, *440*, 357–361. [CrossRef]
41. Luo, W.; Wang, J.; Stewart, K.; Clift, M.; Gross, K. Li-Mg-NH: Recent investigations and development. *J. Alloys Compd.* **2007**, *446*, 336–341. [CrossRef]
42. Bogdanovic, B.; Schwickardi, M. Ti-doped alkali metal aluminium hydrides as potential novel reversible hydrogen storage materials. *J. Alloys Compd.* **1997**, *253*, 1–9. [CrossRef]
43. Ichikawa, T.; Isobe, S.; Hanada, N.; Fujii, H. Lithium nitride for reversible hydrogen storage. *J. Alloys Compd.* **2004**, *365*, 271–276. [CrossRef]
44. Isobe, S.; Ichikawa, T.; Hanada, N.; Leng, H.; Fichtner, M.; Fuhr, O.; Fujii, H. Effect of Ti catalyst with different chemical form on Li-NH hydrogen storage properties. *J. Alloys Compd.* **2005**, *404*, 439–442. [CrossRef]
45. Yao, J.; Shang, C.; Aguey-Zinsou, K.; Guo, Z. Desorption characteristics of mechanically and chemically modified $LiNH_2$ and ($LiNH_2$ + LiH). *J. Alloys Compd.* **2007**, *432*, 277–282. [CrossRef]
46. Chen, Y.; Wang, P.; Liu, C.; Cheng, H.M. Improved hydrogen storage performance of Li-Mg-NH materials by optimizing composition and adding single-walled carbon nanotubes. *Int. J. Hydrog. Energy* **2007**, *32*, 1262–1268. [CrossRef]
47. Janot, R.; Eymery, J.B.; Tarascon, J.M. Investigation of the processes for reversible hydrogen storage in the Li-Mg-NH system. *J. Power Sources* **2007**, *164*, 496–502. [CrossRef]
48. Barison, S.; Agresti, F.; Lo Russo, S.; Maddalena, A.; Palade, P.; Principi, G.; Torzo, G. A study of the $LiNH_2$-MgH_2 system for solid state hydrogen storage. *J. Alloys Compd.* **2008**, *459*, 343–347. [CrossRef]
49. Wang, J.; Liu, T.; Wu, G.; Li, W.; Liu, Y.; Araújo, C.M.; Scheicher, R.H.; Blomqvist, A.; Ahuja, R.; Xiong, Z. Potassium Modified $Mg(NH_2)_2$/2LiH System for Hydrogen Storage. *Angew. Chem. Int. Ed.* **2009**, *48*, 5828–5832. [CrossRef] [PubMed]
50. Ma, L.P.; Wang, P.; Dai, H.B.; Cheng, H.M. Catalytically enhanced dehydrogenation of Li-Mg-NH hydrogen storage material by transition metal nitrides. *J. Alloys Compd.* **2009**, *468*, L21–L24. [CrossRef]
51. Srinivasan, S.S.; Niemann, M.U.; Hattrick-Simpers, J.R.; McGrath, K.; Sharma, P.C.; Goswami, D.Y.; Stefanakos, E.K. Effects of nano additives on hydrogen storage behavior of the complex hydride $LiBH_4/LiNH_2/MgH_2$. *Int. J. Hydrog. Energy* **2010**, *35*, 9646–9652. [CrossRef]

52. Vittetoe, A.W.; Niemann, M.U.; Srinivasan, S.; McGrath, K.; Kumar, A.; Goswami, D.Y.; Stefanakos, E.K.; Thomas, S. Destabilization of $LiAlH_4$ by nanocrystalline MgH_2. *Int. J. Hydrog. Energy* **2009**, *4*, 2333–2339. [CrossRef]
53. Niemann, M.U.; Srinivasan, S.S.; Kumar, A.; Stefanakos, E.K.; Goswami, D.Y.; McGrath, K. Processing analysis of the ternary $LiNH_2$-MgH_2-$LiBH_4$ system for hydrogen storage. *Int. J. Hydrog. Energy* **2009**, *34*, 8086–8093. [CrossRef]
54. Markmaitree, T.; Shaw, L.L. Synthesis and hydriding properties of $Li_2Mg(NH)_2$. *J. Power Sources* **2010**, *195*, 1984–1991. [CrossRef]
55. Varin, R.A.; Zbroniec, L.; Polanski, M.; Bystrzycki, J. A review of recent advances on the effects of microstructural refinement and nano-catalytic additives on the hydrogen storage properties of metal and complex hydrides. *Energies* **2010**, *4*, 1–25. [CrossRef]
56. Bazzanella, N.; Checchetto, R.; Miotello, A. Atoms and nanoparticles of transition metals as catalysts for hydrogen desorption from magnesium hydride. *J. Nanomater.* **2011**. [CrossRef]
57. Kojima, Y.; Kawai, Y.; Ohba, N. Hydrogen storage of metal nitrides by a mechanochemical reaction. *J. Power Sources* **2006**, *159*, 81–87. [CrossRef]
58. Maloney, K.; Dopp, R. *Advanced Materials for Clean Energy Applications*; Online Webinar Event, 26 June 2007; Elsevier: Amsterdam, The Netherlands, 2007.